SCIENCE CHINA
Physics, Mechanics & Astronomy

• Article •

April 2024 Vol. 67 No. 4: 247412
https://doi.org/10.1007/s11433-023-2289-0

Hybridization-mediated quasiparticle and phonon dynamics in single crystal cerium films

Yunhe Pei[1], Yi Wu[2], Kai Hu[1], Zhengxing Wei[1], YiFeng Yang[3,4,5], Yang Liu[2,6], and Jingbo Qi[1*]

[1] *State Key Laboratory of Electronic Thin Films and Integrated Devices, University of Electronic Science and Technology of China, Chengdu 611731, China;*
[2] *Center for Correlated Matter and Department of Physics, Zhejiang University, Hangzhou 310058, China;*
[3] *Beijing National Laboratory for Condensed Matter Physics, Institute of Physics, Chinese Academy of Sciences, Beijing 100190, China;*
[4] *University of Chinese Academy of Sciences, Beijing 100049, China;*
[5] *Songshan Lake Materials Laboratory, Dongguan 523808, China;*
[6] *Collaborative Innovation Center of Advanced Microstructures, Nanjing University, Nanjing 210093, China*

Received September 6, 2023; accepted November 27, 2023; published online March 7, 2024

We report the ultrafast optical pump-probe spectroscopy measurements on the single-crystal cerium films. Our experimental results of temperature-dependent quasiparticle dynamics reveal development of the hybridization between localized f moments and conduction electrons, i.e., evolving from fluctuating hybridization to collective hybridization. Exotic phonon renormalization is discovered to appear at the emerging temperature ($T^{\dagger}$) of fluctuating hybridization apart from its known presence at the coherent temperature (T^{*}), and can hardly be explained by the mean-field theory. The quasiparticle relaxation at high temperatures indicates coexistence of nonthermal electron-electron scattering and inelastic Kondo scattering, while its behavior at low temperatures suggests onset of α phase in the γ-phase dominated film. We also extract the indirect gap below T^{*}, representing the appearance of collective hybridization. Our findings provide novel information about the hybridization and phase evolution in the heavy fermion systems.

cerium, quasiparticle dynamics, hybridization, phonon renormalization

PACS number(s): 71.27.+a, 71.20.Eh, 71.38.-k, 39.30.+w

Citation: Y. Pei, Y. Wu, K. Hu, Z. Wei, Y. F. Yang, Y. Liu, and J. Qi, Hybridization-mediated quasiparticle and phonon dynamics in single crystal cerium films, Sci. China-Phys. Mech. Astron. **67**, 247412 (2024), https://doi.org/10.1007/s11433-023-2289-0

1 Introduction

As a member of rare-earth elements, cerium (Ce) exhibits intricate physical properties and enigmatic underlying physics due to its rich allotropes, as indicated by numerous studies [1-4]. In particular, cerium metal exhibits a γ-α phase transition under modest experimental conditions, which can be achieved by controlling pressure and temperature [5, 6]. Intriguingly, this transition involves a volume collapse of approximately 17% and a magnetic transformation from ferromagnetic to paramagnetic, while maintaining the same lattice symmetry in both phases (face-centred cubic, fcc) [7]. Since the discovery of this isostructural transition, there has been extensive research aimed at explaining its underlying principles [8]. Numerous experimental efforts [9-11] and theoretical studies [12-14] have been undertaken to resolve the puzzle of such phase transition. However, no consensus has been reached within the scientific community, particularly

*Corresponding author (email: jbqi@uestc.edu.cn)

concerning the role of f electrons in the transition.

Several theoretical models have been proposed to understand the role of f electrons in the physical process of the phase transition, which have been partially supported by experimental results. These models suggest a close relationship between the behavior of f electrons and the phase transition, despite differing in their specific explanations [15]. For instance, the Mott transition framework suggests that the phase transition is closely related to the kinetic energy of the $4f$ electron, which remains localized in the γ phase but becomes itinerant in the α phase [16]. On the other hand, the Kondo volume collapse theory proposes that the strength of Kondo hybridization between $4f$ electrons and conducting electrons varies with the phase transition, leading to a rapid change in Kondo temperature (T_K) during the transition [17, 18]. A recent study using angle-resolved photoemission spectroscopy (ARPES) has revealed the possibility of an interplay between the two mechanisms, rather than a mutually exclusive competition [19]. Therefore, it is essential to investigate the behavior of f electrons in this material. Among the available techniques, ultrafast optical pump-probe spectroscopy offers unique advantages for investigating hybridization dynamics in heavy fermion materials, where the f electron plays a crucial role in determining the physical process [20-22].

In this work, we report optical pump-probe measurements on single crystal cerium films. Two kinds of γ-like samples, P1 and P2 as specified in ref. [19], have been investigated. Hybridization processes between the localized f electrons and conduction electrons have been unraveled by investigating the photoexcited quasiparticle dynamics in both samples. Specifically, the initial relaxation rate (Γ) of quasiparticles shows a clear anomaly below the temperature $T^{\dagger}\approx$140 K, and exhibits an apparent fluence dependence for $T < T^*$ (=90±5 K), in contrast to the fluence-independent behavior for $T > T^*$. Such findings suggest the occurrence of a narrow indirect hybridization gap and the existence of precursor hybridization fluctuations in Ce films, similar to the observation in metallic compounds $CeCoIn_5$ and $CeRh_6Ge_4$ [23, 24]. Coherent phonons and their renormalization at different critical temperatures are also observed in Ce films.

2 Experiment and results

The Ce films in our experiments are grown by molecular beam epitaxy (MBE) [19]. After deposition, the films with thickness of ~200 nm were annealed to different temperatures in ultrahigh vacuum and led to two γ-like samples (P1 and P2) with slightly different c lattice constant near the surface regions. Although both phases exhibit strong Kondo hybridization, it was proposed that the slight difference in interlayer spacing leads to Mott-type delocalization of $4f$ electrons [19]. The ultrafast time-resolved differential reflectivity $\Delta R(t)/R$ measurements were performed from 5 K to room temperature using lasers with pulse widths of ~55 and ~67 fs (full width at half maximum, FWHM) at center wavelengths of 800 and 1030 nm, respectively.

2.1 Dynamics of P1 film

Transient reflectivity $\Delta R(t)/R$ signals of P1 film are shown in Figure 1(a). An instantaneous rise is observed after photoexcitation at all temperatures. The temporal evolution of $\Delta R(t)/R$ within the initial several picoseconds (ps) is typically attributed to scattering processes of electron-electron (e-e) and electron-boson in strongly correlated systems [25, 26]. The bosonic excitations involved in these interactions may include phonons or other bosonic modes [27, 28]. As shown in Figure 1(b), a prominent fluence-dependent behavior is observed in the initial decay. To obtain the quantitative information on the quasiparticle relaxation, we fit the experimental data using a single exponential function, $\Delta R/R = Ae^{-\Gamma t}$. Here, A and Γ are the amplitude and decay rate, respectively. The extracted Γ as a function of temperature under various pump fluences are shown in Figure 1(c). Within the experimental errors, Γ shows a clear fluence-dependence behavior below a critical temperature of T^* (=90±5 K).

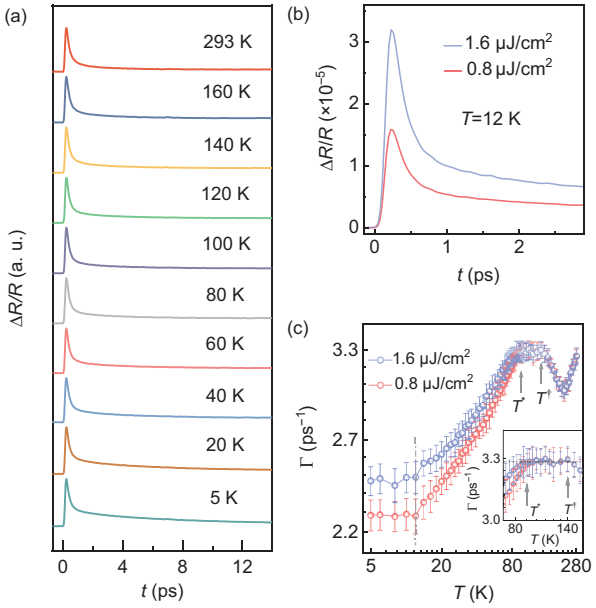

Figure 1 (Color online) (a) Time-resolved differential reflectivity $\Delta R(t)/R$ of the P1 cerium film as a function of temperature. (b) $\Delta R(t)/R$ at 12 K under different pump fluences. (c) The decay rate Γ as a function of temperature at pump fluences of 0.8 and 1.6 μJ/cm^2, respectively. The insert shows Γ between T^* and $T^{\dagger}$.

Such fluence-dependent behavior in the heavy-fermion systems can be explained by Rothwarf-Taylor (RT) model [29-31], where the dynamics of quasiparticles (n) and bosons (N) are highly influenced by the emergence of a narrow energy gap in the density of states (DOS). Mathematically, the RT model describes two coupled nonlinear-differential equations that capture the time-evolution of number of quasiparticles and bosons [29]:

$$\frac{\mathrm{d}n}{\mathrm{d}t} = \beta N - Rn^2, \tag{1}$$

$$\frac{\mathrm{d}N}{\mathrm{d}t} = \frac{1}{2}\left[Rn^2 - \beta N\right] - (N - N_T)\,\tau_\Gamma^{-1}, \tag{2}$$

where n is the total number of quasiparticles, R represents the recombination coefficient of quasiparticles, N is the density of bosons with energy larger than 2Δ (Δ is the energy gap), β is the transition probability for regenerating excited quasiparticles by high frequency bosons, τ_Γ^{-1} is the escaping rate of the high frequency bosons, and N_T is the density of thermal equilibrium bosons. In the above equations, when the escaping rate τ_Γ^{-1} is large, a bimolecular recombination term then will dominate the quasiparticle relaxation, causing a nonlinear Rn^2 contribution and hence the strong fluence-dependence of Γ [23, 28].

According to RT model, upon formation of the narrow energy gap, the decay rate of quasiparticles, Γ, and the density of thermally excited quasiparticles, n_T, can be described by the following equations [32, 33]:

$$\Gamma(T) \propto \left[\frac{\delta}{\zeta n_T + 1} + 2n_T\right]\left(\Delta + \Lambda T\Delta^4\right), \tag{3}$$

$$n_T(T) = \frac{A(0)}{A(T)} - 1 \propto (T\Delta)^p\, \mathrm{e}^{-\Delta/T}, \tag{4}$$

where δ, ζ and Λ are fitting parameters, respectively, Δ is the energy gap, p ($0 < p < 1$) is a constant that is determined by the shape of the gapped DOS [31, 34]. We use eq. (4) to fit our data, and the best fit (Figure 2) is obtained for an energy gap of ~4 meV and $p = 0.27$.

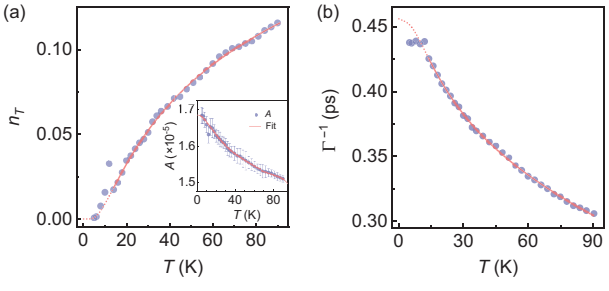

Figure 2 (Color online) Fitting results of the data from the P1 cerium film. (a) The density of thermally excited quasiparticles n_T as a function of temperature below T^*. The inset shows the temperature-dependent amplitude A. (b) Decay time Γ^{-1} as a function of temperature below T^*. Values of A and Γ^{-1} here are derived from measurements conducted at the pump fluence of 0.8 μJ/cm^2. The red curves are the fitting results using the RT model.

Above the critical temperature T^*, the decay rate (Γ) exhibits a fluence-independent behavior, as shown in Figure 1(c). Upon raising the temperature, Γ initially is almost unchanged, and subsequently decreases above $T^\dagger$. As the temperature continues to rise, Γ passes a local minima and then undergoes an obvious increase. For the T-dependence of Γ above $T^\dagger$, both two temperature model (TTM) [35, 36] and the nonequilibrium model (NEM) [25] are inapplicable, since the fluence-independence rules out the feasibility of TTM and behavior of $\Gamma(T)$ from $T^\dagger$ to room temperature contradicts the predictions made by NEM (see sect. 3 for more details).

We now focus on the oscillatory components in the $\Delta R/R$ signals, which were extracted from the decay processes by subtracting the exponential fitting curves of $\Delta R(t)/R$, as shown in Figure 3(a) and (b) (see Supplemental Material for more data). Three obvious terahertz (THz) modes are

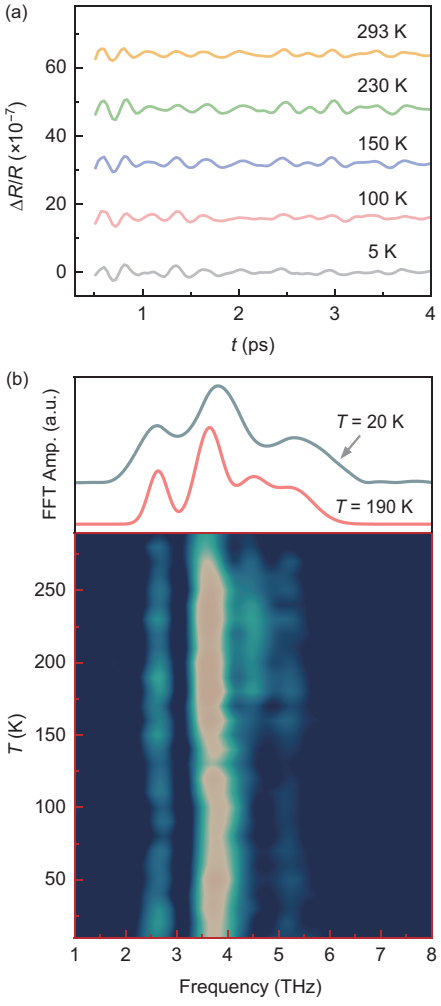

Figure 3 (Color online) (a) Extracted oscillation components at some typical temperatures (5, 100, 150, 230 and 293 K). (b) The Fourier transform spectra in the frequency domain for oscillations from room temperature down to 5 K.

observed at all measured temperatures including f_1~2.6 THz, f_2~3.7 THz and f_3~5.2 THz. The mode with a frequency of ~4.4 THz is only observed above $T^\dagger$. To study the oscillations quantitatively, we fit the oscillations in frequency-domain via several Gaussians (see Supplemental Material for more details). The derived temperature-dependent evolution of f_j is shown in Figure 4. We can see anomalies emerging at temperatures T^* and $T^\dagger$. In general, the oscillations with THz frequency originate from the coherent optical phonons [37], initiated either through the displacive excitations or the coherent Raman process [38, 39].

Evolution of the phonon energies in the temperature domain generally can be described by the anharmonic phonon model [40-43]:

$$\omega^{ph\text{-}ph} = \omega_0 + a_1\left[1 + 2n_B(\frac{\omega_0}{2}, T)\right] + a_2\left[1 + 3n_B(\frac{\omega_0}{3}, T) + 3n_B^2(\frac{\omega_0}{3}, T)\right], \quad (5)$$

where ω_0 is the intrinsic frequency, a_1 and a_2 are the fitting parameters. $n_B(\omega, T) = [\exp(\hbar\omega/k_BT) - 1]^{-1}$ is the Bose-Einstein distribution function. The fitting results are shown in Figure 4. For f_1 and f_2, the data below $T^\dagger$ deviate from the prediction by the anharmonic phonon model manifested by hardening effect, although a reasonable agreement exists at temperatures $T > T^\dagger$. The hardening behavior below temperature $T^\dagger$ is first observed in the heavy fermion system. Anomalous T-dependent behavior is also observed below T^*, and is similar with previous findings around this temperature [23, 24]. Such new finding demonstrates that phonon renormalization can not only happen below the collective hybridization, but also appear with the emergence of hybridization fluctuation. Unfortunately, the mean-field theory involving the Kondo singlets could not be used to describe the behavior below $T^\dagger$ and T^* anymore. T-dependent f_3 shows anomaly around T^*, and is difficult to understand by any existing models. f_4 phonon mode appears above $T^\dagger$, and its origin is not clear at this stage. However, it may be related to the nonthermal and inelastic Kondo scattering processes discussed below, since it shows anomalous change around a similar temperature 225 K with that of $\Gamma(T)$ at $T > T^\dagger$.

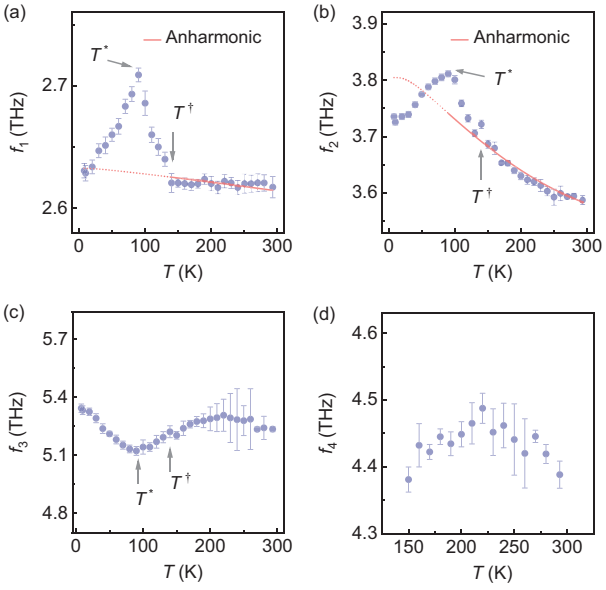

Figure 4 (Color online) The temperature-dependent evolution of oscillations with frequencies of (a) f_1, (b) f_2, (c) f_3 and (d) f_4, respectively. The red lines in (a) and (b) are the fitting curves with anharmonic model.

2.2 Dynamics of P2 film

Similar to the P1 sample, typical transient reflectivity $\Delta R(t)/R$ data of the P2 film are shown in Figure 5(a). There exist some differences of the shape between signals in Figures 1(a) and 5(a). This is understandable since these two samples have undergone different annealing processes, whose influence on the electronic and structural properties are different, and hence lead to various scattering processes. After photoexcitation, the instantaneous rise can also be seen in the signals at all investigated temperatures and the fluence-dependent decay rate is observed again (Figure 5(b)). By using the same method of data analysis as that employed for the P1 sample, the extracted decay rates under different pump fluences as a function of temperature are shown in Figure 5(c). Two critical temperatures (T^* and $T^\dagger$) can also be

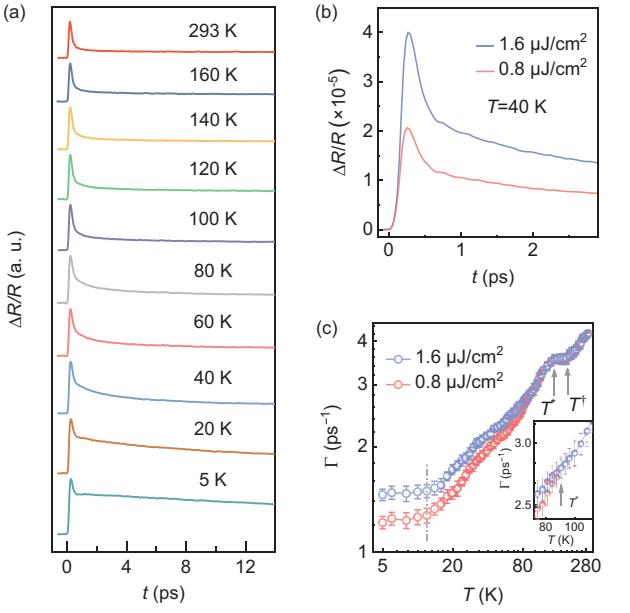

Figure 5 (Color online) (a) Time-resolved differential reflectivity $\Delta R(t)/R$ of the P2 cerium film as a function of temperature. (b) $\Delta R(t)/R$ signals of P2 cerium film at 40 K under different pump fluences. (c) The decay rate as a function of temperature at pump fluences of 0.8 and 1.6 μJ/cm^2, respectively. The insert shows Γ between 70 and 120 K.

extracted, and are nearly the same as those for the P1 sample.

The fluence-dependent Γ below T^* can be fitted well by the RT model, as shown in Figure 6, yielding a narrow energy gap of 2Δ ~7 meV with p≈0.9. It should be noted that various p values in P1 and P2 samples may suggest that the shapes of DOS are different [34]. In the temperature range $T > T^*$, the absence of fluence-dependence indicates the vanishing of hybridization gap. As the temperature increases, the relaxation rate shows a similar T-dependent behavior as that of the P1 sample, although there exists some difference between them. Clearly, such T-dependence also cannot be explained by TTM or NEM (see sect. 3 for detailed discussion).

Same to the P1 film, oscillatory components with THz frequency are also observed in the $\Delta R(t)/R$ signals of the P2 sample (Figure 7). To study them quantitatively, we fitted the data using damped oscillations:

$$(\Delta R/R)_{\rm osc} = \sum_{j=1,2} A_j e^{-\Gamma'_j t} \sin(\Omega_j t + \phi_j), \quad (6)$$

where A_j, Γ'_j, Ω_j, and ϕ_j are the amplitude, damping rate, frequency, and phase, respectively. The derived temperature evolution of f_j (=$\Omega_j/2\pi$) are shown in Figure 7(c) and (d).

The f_1 mode maintains nearly unchanged below T^*, while a downturn can be seen at the temperature region below T^* for the f_2 mode. The modes f_1 and f_2 show a good consistence with the anharmonic phonon model at the temperature above $T^\dagger$ and T^*, respectively. The hardening of f_1 mode below $T^\dagger$ is noticeable, and is similar with the observation in P1 sample. Compared with the f_1 mode, f_2 phonon frequency below T^* can be well described by the Kondo-phonon coupling via the mean-field theory.

3 Discussion

Investigation of the decay processes in two types of cerium films has revealed a two-stage scenario for the hybridization

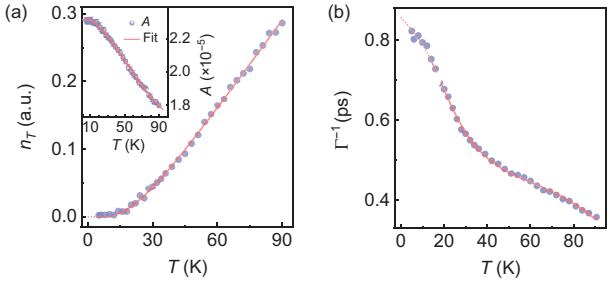

Figure 6 (Color online) Fitting results of the P2 cerium film. (a) The density of thermally excited quasiparticles n_T as a function of temperature below T^*. The inset illustrates the temperature-dependent amplitude A. (b) Γ^{-1} as a function of temperature below T^*. The pump fluence is 0.8 μJ/cm^2.

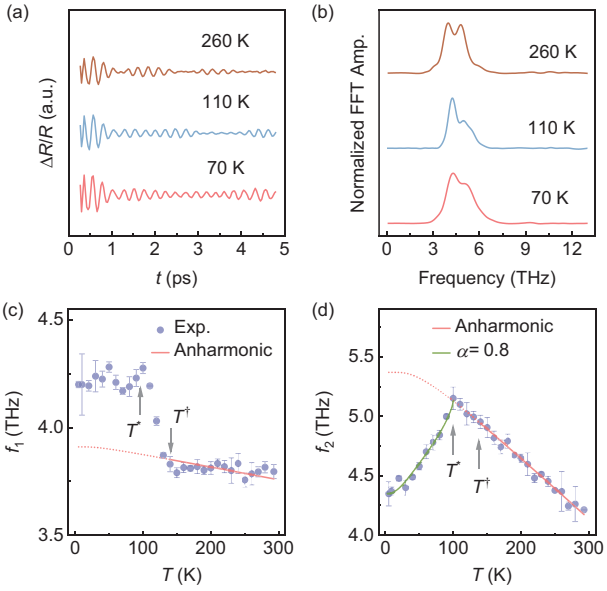

Figure 7 (Color online) (a) Extracted oscillating components at representative temperatures (70, 110 and 260 K). (b) Oscillatory signals in frequency domain obtained through the fast Fourier transform (FFT). Two modes are found. The temperature-dependent evolution of oscillations with frequencies of (c) f_1 and (d) f_2, respectively. The red lines in both (c) and (d) are the fitting results using the anharmonic phonon model. The green line in (d) is the fitting curve taking into consideration the contribution of Kondo singlets, yielding α = 0.8, more details about fitting can be seen in ref. [23].

dynamics. The critical temperature $T^\dagger$~140 K marks the temperature below, which emerges the hybridization between localized f electrons and conducting electrons, while a coherent hybridization state has not formed within the entire lattice. Below the critical temperature T^*, there appears further development of such hybridization into a coherent heavy electron state associated with the formation of a narrow indirect hybridization gap in DOS.

Above T^*, as observed in both P1 and P2, the fluence-independent behavior of Γ indicates that the relaxation dynamics of quasiparticles is not dominated by TTM, but may potentially involve a nonthermal process [25, 36], where the relaxation through *e-e* collisions is comparable with electron-boson scatterings [23]. This observation implies that the relaxation time due to *e-e* collisions is longer than the *e-ph* relaxation time ($\tau_{e\text{-}e} > \tau_{e\text{-}ph}$). Between T^* and $T^\dagger$, the presence of plateau in the T dependence of Γ reveals a more pronounced photoinduced nonthermal effect in the P1 film compared with the P2 film. Γ(T) observed in the P2 sample below $T^\dagger$ suggests the possible coupling between fluctuating f moments and nonequilibrium electrons near E_F, suppressing *e-e* scatterings. A similar phenomenon has also been reported in other heavy fermion compounds [23, 24].

Above $T^\dagger$, Γ exhibits clear minimums as temperature increases (~220 K for P1, ~190 K for P2). It is obvious that TTM fails to account for this behavior. According to NEM,

the decay rate is indeed fluence-independent, but NEM predicts that the decay rate should follow a $1/T$ dependence [25], which is also not consistent with our results. Thus, the temperature dependence of decay rate Γ for both P1 and P2 samples cannot be fully explained by a single mechanism.

It is reasonable to propose that the quasiparticle dynamics in this temperature range could be a result of two competing mechanisms. One is the nonthermal process, and the other is possibly the inelastic Kondo scattering between conduction electrons and localized magnetic moments [44]. Therefore, the evolution of $\Gamma(T)$ can be described by the expression $\Gamma = 1/\tau = A/T + B\ln T + C$, where the term A/T corresponds to the nonthermal process, the term $\ln T$ represents the inelastic Kondo scattering process [44], and C is a temperature-independent offset. The fitting results are depicted in Figure 8, demonstrating a good consistency with the experimental data. This implies that the dynamics observed within this temperature range are governed by the interplay between two mechanisms. Such a competitive relationship has also been reported in the Ce-based heavy fermion compounds [44-46]. It should be emphasized that the correlation strength manifested by *e*-*e* interaction and electron-phonon (or electron-boson) coupling should be different between these two samples. Based on our fitting, the parameter A of sample P1 increases nearly by 20% compared with that of sample P2. Meanwhile, the parameter B between these two samples only has a tiny relative change, i.e., ~4%. Such a result indicates a larger nonthermal effect observed in P1 film, where there should appear a stronger correlation effect.

We observed four phonon modes in sample P1 and two phonon modes in sample P2. For the two modes with relatively higher frequency (f_1 and f_2 modes of P2, f_3 and f_4 modes of P1), their corresponding differences between these two samples are not significant (~6%). This is reasonable because the annealing temperatures for sample P1 and sample P2 were quite different during the sample growth. However, the low-frequency modes in sample P2 were not detected, possibly due to their related signals being too small and exceeding our detection limit.

The anomalies of phonon energy observed around T^* for both samples can be attributed to the coupling between coherent heavy electrons and phonons. This phenomenon has been previously reported in Ce-based compounds [23, 24]. However, by contrast to those phonon modes in P1, the T-dependent f_2 mode in P2 below T^* can be well modeled by the mean-field theory. Such difference might be attributed to the stronger correlation effect present in P1, due to its essential role in the intricate electron-phonon coupling. On the other hand, absence of any evidence of structural changes near $T^\dagger$, as determined by X-ray diffraction (XRD) measurements [19], suggests that the anomalies of phonon frequency near $T^\dagger$ are likely induced by the *c*-*f* hybridization fluctuations, as shown in Figure 7(c). Such phonon renormalization near $T^\dagger$ is observed for the first time [23, 24]. New theoretical model is required to explain the phonon hardening effect below $T^\dagger$.

We also compare the critical temperatures obtained in our pump-probe experiment with those in other measurements. For example, the resistance of P1 sample obtained from the electrical transport is shown in Figure 9. According to the resistance data, the broad peak at around 90 K confirms that the coherent temperature T^* is consistent with the result from pump-probe technique in this work. The $T^\dagger$ can be extracted from the derivative of resistance (Figure 9(b)), and agrees well with our data within the experimental uncertainty. In addition, the sharp peak at 12 K is believed to originate from the γ-α phase transition, which has been confirmed by the T-dependent XRD measurement [19]. In our pump-probe experiments, we observed that quasiparticle scattering rate stops decreasing below ~12 K, as seen in Figure 1(c). Similar phenomenon is also seen in the P2 sample. This behavior suggests some change of bosonic excitations involving with the quasiparticle scatterings around this temperature. Theoretical calculations have revealed that the α-Ce has a much larger phonon density of states, especially in the high-frequency region compared with that of γ-Ce [14]. This

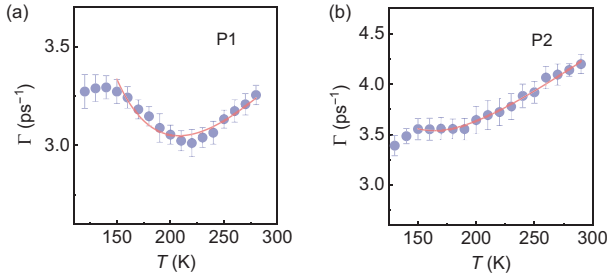

Figure 8 (Color online) Γ of (a) P1 and (b) P2 in high temperature regions at a fluence of 0.8 μJ/cm^2, respectively. The red line is the fitting curve using the model described in the main text.

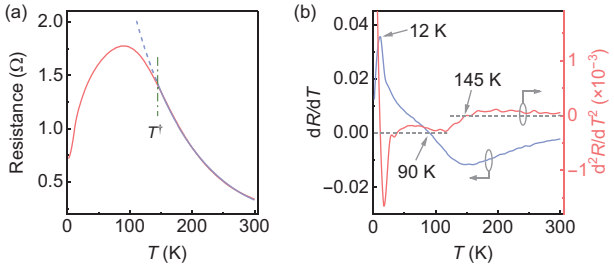

Figure 9 (Color online) (a) Transport measurement of cerium film with P1 phase. The blue line shows the fitting curve in the high temperature range ($T > T^\dagger$) using equation $R(T) \propto \rho(T) = a + b \cdot T + c \cdot \ln T$ [44]. (b) First and second derivative of the resistance with respective to the temperature T for P1 sample.

result implies that if there is a phase transition from γ to α below 12 K, the electron-phonon scattering process will prevent $\Gamma(T)$ from further reduction as T decreases. In fact, the temperature-dependent XRD experiments already indicate that some portion of the film has converted into the α phase, although it is a very small percentage of ~1%. Therefore, our findings illustrate that the quasiparticle relaxation is very sensitive to the structural changes.

Finally, oscillations with gigahertz (GHz) frequency are observed in the long decay process of both samples. This type of oscillation generally arises from the transient stress due to absorption of ultrafast pump pulse at the surface of sample [47, 48]. Such stress could induce a strain wave that propagates deep into the sample along the normal of surface. This strain wave is also known as coherent longitudinal acoustic phonon, whose associated frequency of the oscillation depends on the probing wavelength [49,50] (see the Supplemental Material for more details). Based on the relevant data, we can obtain the speed of sound at room temperature for both samples, which are ~1.37 km/s for P1 cerium film and ~3.72 km/s for P2 cerium film, respectively. They are consistent with the value (~2.4 km/s) in bulk cerium sample [51, 52]. Their difference may reflect the difference of lattice and electronic properties between these two samples, caused by the different annealing procedures.

4 Conclusion

In summary, we investigate the hybridization process in two types of single-crystal cerium films over a wide temperature range. The relaxation rate below $T^{\dagger}$~140 K suggests the possibility of "band bending" already in this high temperature region, as previously detected in the ARPES experiments [11, 15, 53]. Below a coherence temperature T^{*}~90 K, we observe an indirect band gap for both samples, which protects the coherent heavy electron state. The associated anomalies in the phonon frequencies demonstrate that the hybridization between local f moments and conducting electrons significantly affects the interaction among phonons, although the existing model of Kondo-phonon coupling fails to understand the strange T-dependent behavior below $T^{\dagger}$ and T^{*}. The observed two-stage hybridization process is in close resemblance to that in other Ce-based heavy fermion compounds [54, 55], for instance, $CeRh_6Ge_4$ and $CeCoIn_5$. This similarity implies that the hybridization process of f electrons shows a universal physical mechanism that is from the intrinsic nature of f electrons. In addition, we also find the quasiparticle relaxation is very sensitive to the γ-α phase transitions. This may provide an alternative perspective for studying the relation between mysterious γ-α isostructural transition and the temperature-dependent physical nature of f electrons in cerium. Finally, (1) it remains open how the hybridization process changes with the phase transition under external pressure; (2) our experiment demonstrates, in general, that new theory must be needed to explain renormalization of the phonon energy upon emergence of hybridization.

This work was supported by the National Key Research and Development Program of China (Grant Nos. 2022YFA1403000, and 2022YFA1402200), the National Natural Science Foundation of China (Grant Nos. 92365102, 11974070, 11734006, 11925408, 11921004, 12004067, 62027807, and 12174331), and the Frontier Science Project of Dongguan (Grant No. 2019622101004).

Conflict of interest The authors declare that they have no conflict of interest.

Supporting Information

The supporting information is available online at http://phys.scichina.com and https://link.springer.com. The supporting materials are published as submitted, without typesetting or editing. The responsibility for scientific accuracy and content remains entirely with the authors.

1 N. Lanatá, Y. X. Yao, C. Z. Wang, K. M. Ho, J. Schmalian, K. Haule, and G. Kotliar, Phys. Rev. Lett. **111**, 196801 (2013), arXiv: 1305.3950.
2 M. J. Lipp, D. Jackson, H. Cynn, C. Aracne, W. J. Evans, and A. K. McMahan, Phys. Rev. Lett. **101**, 165703 (2008).
3 A. V. Nikolaev, and A. V. Tsvyashchenko, Phys.-Usp. **55**, 657 (2012), arXiv: 1210.5895.
4 I. Loa, E. I. Isaev, M. I. McMahon, D. Y. Kim, B. Johansson, A. Bosak, and M. Krisch, Phys. Rev. Lett. **108**, 045502 (2012).
5 M. Krisch, D. L. Farber, R. Xu, D. Antonangeli, C. M. Aracne, A. Beraud, T. C. Chiang, J. Zarestky, D. Y. Kim, E. I. Isaev, R. Ahuja, and B. Johansson, Proc. Natl. Acad. Sci. U.S.A. **108**, 9342 (2011).
6 I. K. Jeong, T. W. Darling, M. J. Graf, T. Proffen, R. H. Heffner, Y. Lee, T. Vogt, and J. D. Jorgensen, Phys. Rev. Lett. **92**, 105702 (2004), arXiv: cond-mat/0308416.
7 S. Eryigit, C. Parlak, and R. Eryigit, J. Phys.-Condens. Matter **34**, 295402 (2022).
8 A. W. Lawson, and T. Y. Tang, Phys. Rev. **76**, 301 (1949).
9 D. M. Wieliczka, C. G. Olson, and D. W. Lynch, Phys. Rev. Lett. **52**, 2180 (1984).
10 F. Patthey, B. Delley, W. D. Schneider, and Y. Baer, Phys. Rev. Lett. **58**, 1283 (1987).
11 X. G. Zhu, Y. Liu, Y. W. Zhao, Y. C. Wang, Y. Zhang, C. Lu, Y. Duan, D. H. Xie, W. Feng, D. Jian, Y. H. Wang, S. Y. Tan, Q. Liu, W. Zhang, Y. Liu, L. Z. Luo, X. B. Luo, Q. Y. Chen, H. F. Song, and X. C. Lai, NPJ Quant. Mater. **5**, 47 (2020), arXiv: 1911.10722.
12 R. Ramirez, and L. M. Falicov, Phys. Rev. B **3**, 2425 (1971).
13 A. K. McMahan, K. Held, and R. T. Scalettar, Phys. Rev. B **67**, 075108 (2003), arXiv: cond-mat/0208443.
14 L. Huang, and C. A. Chen, J. Phys.-Condens. Matter **19**, 476206 (2007).
15 Q. Y. Chen, W. Feng, D. H. Xie, X. C. Lai, X. G. Zhu, and L. Huang, Phys. Rev. B **97**, 155155 (2018).
16 B. Johansson, Philos. Mag. **30**, 469 (1974).
17 J. W. Allen, and R. M. Martin, Phys. Rev. Lett. **49**, 1106 (1982).
18 J. W. Allen, and L. Z. Liu, Phys. Rev. B **46**, 5047 (1992).
19 Y. Wu, Y. Fang, P. Li, Z. Xiao, H. Zheng, H. Yuan, C. Cao, Y. Yang, and Y. Liu, Nat. Commun. **12**, 2520 (2021), arXiv: 2103.05848.
20 J. Demsar, R. D. Averitt, K. H. Ahn, M. J. Graf, S. A. Trugman, V. V.

Kabanov, J. L. Sarrao, and A. J. Taylor, Phys. Rev. Lett. **91**, 027401 (2003), arXiv: cond-mat/0305597.
21 E. E. M. Chia, D. Talbayev, J. X. Zhu, H. Q. Yuan, T. Park, J. D. Thompson, C. Panagopoulos, G. F. Chen, J. L. Luo, N. L. Wang, and A. J. Taylor, Phys. Rev. Lett. **104**, 027003 (2010).
22 J. Qi, T. Durakiewicz, S. A. Trugman, J. X. Zhu, P. S. Riseborough, R. Baumbach, E. D. Bauer, K. Gofryk, J. Q. Meng, J. J. Joyce, A. J. Taylor, and R. P. Prasankumar, Phys. Rev. Lett. **111**, 057402 (2013), arXiv: 1303.2694.
23 Y. P. Liu, Y. J. Zhang, J. J. Dong, H. Lee, Z. X. Wei, W. L. Zhang, C. Y. Chen, H. Q. Yuan, Y. Yang, and J. Qi, Phys. Rev. Lett. **124**, 057404 (2020), arXiv: 1906.07990.
24 Y. H. Pei, Y. J. Zhang, Z. X. Wei, Y. X. Chen, K. Hu, Y. Yang, H. Q. Yuan, and J. Qi, Phys. Rev. B **103**, L180409 (2021), arXiv: 2102.08572.
25 C. Gadermaier, A. S. Alexandrov, V. V. Kabanov, P. Kusar, T. Mertelj, X. Yao, C. Manzoni, D. Brida, G. Cerullo, and D. Mihailovic, Phys. Rev. Lett. **105**, 257001 (2010), arXiv: 0902.1636.
26 D. N. Basov, R. D. Averitt, D. van der Marel, M. Dressel, and K. Haule, Rev. Mod. Phys. **83**, 471 (2011), arXiv: 1106.2309.
27 M. C. Wang, H. S. Yu, J. Xiong, Y. F. Yang, S. N. Luo, K. Jin, and J. Qi, Phys. Rev. B **97**, 155157 (2018).
28 C. Giannetti, M. Capone, D. Fausti, M. Fabrizio, F. Parmigiani, and D. Mihailovic, Adv. Phys. **65**, 58 (2016), arXiv: 1601.07204.
29 A. Rothwarf, and B. N. Taylor, Phys. Rev. Lett. **19**, 27 (1967).
30 V. V. Kabanov, J. Demsar, and D. Mihailovic, Phys. Rev. Lett. **95**, 147002 (2005), arXiv: cond-mat/0501711.
31 J. Demsar, J. L. Sarrao, and A. J. Taylor, J. Phys.-Condens. Matter **18**, R281 (2006).
32 E. E. M. Chia, J. X. Zhu, H. J. Lee, N. Hur, N. O. Moreno, E. D. Bauer, T. Durakiewicz, R. D. Averitt, J. L. Sarrao, and A. J. Taylor, Phys. Rev. B **74**, 140409 (2006), arXiv: cond-mat/0605240.
33 E. E. M. Chia, J. X. Zhu, D. Talbayev, R. D. Averitt, A. J. Taylor, K. H. Oh, I. S. Jo, and S. I. Lee, Phys. Rev. Lett. **99**, 147008 (2007), arXiv: 0705.1724.
34 J. Demsar, V. K. Thorsmølle, J. L. Sarrao, and A. J. Taylor, Phys. Rev. Lett. **96**, 037401 (2006), arXiv: cond-mat/0512108.
35 P. B. Allen, Phys. Rev. Lett. **59**, 1460 (1987).
36 R. H. M. Groeneveld, R. Sprik, and A. Lagendijk, Phys. Rev. B **51**, 11433 (1995).
37 Z. Wei, S. Zhang, Y. Su, L. Cheng, H. Zhou, Z. Jiang, H. Weng, and J. Qi, Sci. China-Phys. Mech. Astron. **65**, 257012 (2022), arXiv: 2107.12748.
38 G. A. Garrett, T. F. Albrecht, J. F. Whitaker, and R. Merlin, Phys. Rev. Lett. **77**, 3661 (1996).
39 R. Merlin, Solid State Commun. **102**, 207 (1997).
40 L. Cheng, F. C. Fei, H. Hu, Y. M. Dai, F. Q. Song, and J. Qi, Phys. Rev. B **106**, 104308 (2022).
41 J. Menéndez, and M. Cardona, Phys. Rev. B **29**, 2051 (1984).
42 T. R. Hart, R. L. Aggarwal, and B. Lax, Phys. Rev. B **1**, 638 (1970).
43 C. Zhang, Q. Y. Wu, W. S. Hong, H. Liu, S. X. Zhu, J. J. Song, Y. Z. Zhao, F. Y. Wu, Z. T. Liu, S. Y. Liu, Y. H. Yuan, H. Huang, J. He, S. Li, H. Y. Liu, Y. X. Duan, H. Q. Luo, and J. Q. Meng, Sci. China-Phys. Mech. Astron. **65**, 237411 (2022), arXiv: 2109.06460.
44 D. Kaczorowski, A. P. Pikul, D. Gnida, and V. H. Tran, Phys. Rev. Lett. **103**, 027003 (2009).
45 L. Wang, Z. Fu, J. Sun, M. Liu, W. Yi, C. Yi, Y. Luo, Y. Dai, G. Liu, Y. Matsushita, K. Yamaura, L. Lu, J. G. Cheng, Y. Yang, Y. Shi, and J. Luo, NPJ Quant. Mater. **2**, 36 (2017), arXiv: 1608.07013.
46 E. Bauer, R. Hauser, E. Gratz, K. Payer, G. Oomi, and T. Kagayama, Phys. Rev. B **48**, 15873 (1993).
47 C. Thomsen, H. T. Grahn, H. J. Maris, and J. Tauc, Phys. Rev. B **34**, 4129 (1986).
48 L. Cheng, C. La-o-vorakiat, C. S. Tang, S. K. Nair, B. Xia, L. Wang, J. X. Zhu, and E. E. M. Chia, Appl. Phys. Lett. **104**, 211906 (2014).
49 J. Qi, J. A. Yan, H. Park, A. Steigerwald, Y. Xu, S. N. Gilbert, X. Liu, J. K. Furdyna, S. T. Pantelides, and N. Tolk, Phys. Rev. B **81**, 115208 (2010), arXiv: 0807.1740.
50 J. K. Miller, J. Qi, Y. Xu, Y. J. Cho, X. Liu, J. K. Furdyna, I. Perakis, T. V. Shahbazyan, and N. Tolk, Phys. Rev. B **74**, 113313 (2006), arXiv: cond-mat/0701226.
51 R. S. Hixson, B. M. La Lone, M. D. Staska, G. D. Stevens, W. D. Turley, and L. R. Veeser, J. Appl. Phys. **129**, 155106 (2021).
52 M. V. Zhernokletov, A. E. Kovalev, V. V. Komissarov, M. G. Novikov, M. A. Zocher, and F. J. Cherne, J. Phys.-Conf. Ser. **121**, 072003 (2008).
53 F. Schiller, M. Heber, V. D. P. Servedio, and C. Laubschat, Phys. Rev. B **68**, 233103 (2003).
54 Y. Liu, Sci. China-Phys. Mech. Astron. **64**, 127431 (2021).
55 J. Wang, and Y. F. Yang, Sci. China-Phys. Mech. Astron. **65**, 257211 (2022), arXiv: 2112.14515.